Available online at www.sciencedirect.com
ScienceDirect
Catalysis Today 133–135 (2008) 743–749
CATALYSIS TODAY
www.elsevier.com/locate/cattod

Selective CO oxidation in excess of H_2 over high-surface area CuO/CeO_2 catalysts

Antonio Gómez-Cortés [a,b], Yasser Márquez [a], Jesús Arenas-Alatorre [a], Gabriela Díaz [a,*]

[a] *Instituto de Física, Universidad Nacional Autónoma de México, Apdo. Postal 20-364, México, D.F. C.P. 01000, México*
[b] *Fac. de Química, UAEM Toluca Estado de México C.P. 50120, México*

Available online 31 January 2008

Abstract

The influence of the surface area, crystal size of the support and the Cu loading (3–9 wt.%) on the catalytic behavior of CuO/CeO_2 catalysts was investigated in the preferential CO oxidation (PROX) reaction. Two ceria samples were used: a high-surface area one (SCe) prepared by the templating technique and a low surface commercial one (ACe). Copper was incorporated to the calcined support by classical impregnation. Techniques were used to characterize the textural, structural and chemical properties of the catalysts (BET, XRD, HRTEM, and TPR). For catalysts supported on SCe these techniques evidenced highly dispersed copper species in strong interaction with nanosized CeO_2 crystals. The enhanced redox properties of the CuO–support interface sites at low temperature evidenced by TPR in CuSCe catalysts play a fundamental role in the catalytic behavior for the CO oxidation in presence of excess H_2 (PROX). CuSCe catalysts showed excellent catalytic activity compared to catalysts supported on the commercial CeO_2. Total conversion of CO is obtained at 125 °C with 100% selectivity to CO_2. In the presence of CO_2 and H_2O the maximum CO conversion for temperatures higher than 125 °C was 95%. Selectivity also decreased being more pronounced when H_2O was present. This negative effect was reversible since the original activity and selectivity were practically restored upon elimination of these components from the feed. Partially reduced Cu^+ species seem to be present in the catalysts according to CO adsorption followed by DRIFT.

Keywords: Nanosized CeO_2; CuO/CeO_2; CO oxidation; PROX

1. Introduction

Among systems of environmentally friendly energy generation, fuel cells development has increased in the last years [1,2]. H_2-fueled polymer electrolyte membrane fuel cells (H_2-PEMFC) are very attractive for small scale and automotive applications [3]. The H_2 fuel is usually generated by steam reforming of hydrocarbons or alcohols followed by the WGS reaction [4]. The typical composition of effluents coming from such processes contains about 1% of CO in a large excess of H_2, the CO being a poison to the Pt electrode in the PEMFC. Thus, further purification of the H_2 is needed to reduce the CO concentration below 10 ppm. The available methods include the selective catalytic oxidation of CO in presence of H_2 (reaction 1), also known as preferential CO oxidation (PROX). The goal in this reaction is the oxidation of CO to CO_2 without simultaneously oxidizing H_2 to H_2O. The $H_2 + O_2$ reaction is more exothermic and, hence, favored at high temperatures. Selective catalysts active at low temperatures and stable towards deactivation by CO_2 and H_2O present in the feed are needed.

$$CO + \tfrac{1}{2}O_2 + H_2 \rightarrow CO_2 + H_2 \quad (1)$$

The PROX reaction has been extensively investigated [5–11]. Supported Pt group metals [12–14] have been studied for this reaction. More recently, small supported Au particles (<5 nm) have shown better activity than Pt catalysts in particular at low temperatures <120 °C [6,7]. Application of noble metals is nevertheless limited due to their high selectivity for H_2 oxidation above 100 °C.

An alternative to noble metal catalysts is the copper based catalysts, in particular the CuO-CeO_2 system. This catalyst has shown good activity in the PROX reaction at low temperature (<120 °C) with an acceptable selectivity to CO_2 [7,15,16] and tolerance to the presence of CO_2 and H_2O in the feed [15,16]. In

* Corresponding author. Tel.: +5255 56225097; fax: +5255 56225008.
E-mail address: diaz@fisica.unam.mx (G. Díaz).

0920-5861/$ – see front matter
doi:10.1016/j.cattod.2007.12.083

addition the low cost of the copper compared to the noble metals promotes the research on this area.

On their side, cerium based materials have important applications in areas such as catalysis, high-temperature ceramics and fuel cells [17,18], among others. The technological importance of ceria is linked to the Ce^{4+}/Ce^{3+} redox couple which allows the material to act as an oxygen buffer by storing and releasing oxygen. The redox and catalytic properties of CeO_2 and related materials are linked to the crystal size and to structural defects as oxygen vacancies. In particular, it has been reported [19] that for CeO_2 nanocrystals <10 nm a noticeable increase in the redox properties is observed. In general a decrease in the size of the crystal leads to an augmentation of the surface area and to a change in morphology which provide the appearance of potentially active sites.

For CuO-CeO_2 catalysts, the CO oxidation activity is related to the copper concentration in the catalyst and especially to their state of dispersion [20]. Different preparation methods lead to changes in the dispersion of copper species. Other strategy is to modify the surface area of the support in order to get better dispersion of the copper phase. In this framework the use of templating techniques for the synthesis of mesoporous solids has opened up new opportunities in the design of novel high-surface area materials for catalytic applications.

In this work we studied CuO/CeO_2 materials as catalysts for the selective catalytic oxidation of CO in presence of excess H_2 focusing on the effect of the copper loading and the surface area of the support. High-surface area nanosized CeO_2 crystals were prepared by the templating technique using a non-ionic surfactant and as a reference material a commercial ceria was used.

2. Experimental

2.1. Catalyst preparation

High-surface area CeO_2 was prepared according to the literature following the procedure described by Lyons et al. [21]. Briefly, hexadecylamine (Fluka $C_{16}H_{35}N$) was added to 50% (v/v) water–ethanol solution under stirring for several minutes. A molar ratio inorganic precursor/surfactant equal to two was achieved by adding the required quantity of hydrate cerium(III) acetate (Aldrich, $Ce(C_2H_3O_2)_3xH_2O$) used as precursor of the cerium oxide. This mixture was stirred for 1 h at room temperature and then placed in an oven at 60 °C for 48 h. The precipitate was first washed with water–ethanol solution then filtered and washed again with deionized water. Finally, the solid was dried at 160 °C for 6 h and calcined in air flow at 300 °C for 4 h. As a CeO_2 reference material a commercial CeO_2 from Aldrich calcined at 300 °C was used.

The incorporation of copper was done by classical impregnation using a copper acetate (Aldrich) solution with the adequate concentration to get a nominal copper loading of 3–9 wt.%. After impregnation the materials were dried at 80 °C for 12 h and then calcined in air flow for 2 h at 300 °C.

Hereafter the catalysts are identified as *X*CuSCe and *X*CuACe where *X* indicates the nominal copper loading (3–9 wt.%). SCe (high-surface area one) and ACe (low surface commercial one) stand for the ceria synthesized in this work and the commercial one, respectively.

2.2. Characterization

Textural properties such as specific surface area and total pore volume of the supports and catalysts were determined using a Quantachrome Autosorb equipment with nitrogen gas as adsorbate. The crystalline structure of the solids was studied by X-ray diffraction (XRD) using a Brucker D-8 diffractometer equipped with a Cu Kα radiation source. Diffraction intensity was measured in the 2 theta ranges between 20 and 110°, with a 2 theta step of 0.02° for 8 s per point. The Rietveld technique using FullProf codes [22] was used to refine the ceria crystal structure and to calculate the average crystal size. In addition, characterization of the structure of the catalysts at the nanolevel was performed in a JEOL 2010 FASTEM microscope. The actual copper content of the catalysts was determined by EDX technique. For HRTEM and EDX analysis carbon coated gold grids were used.

Hydrogen temperature programmed reduction (H_2-TPR) experiments were performed in a RIG-100 unit under a flow of 5% H_2/Ar gas mixture (30 cm^3 min^{-1}) and a heating rate of 10 °C min^{-1} from room temperature to 800 °C. The H_2O produced be the reduction process was trapped before the TCD. Prior to TPR runs the samples were pretreated in air flow at 300 °C for 1 h and then cooled to room temperature in argon. Bulk CuO was used as reference for calibration of the TCD signal.

Surface properties of the catalysts were studied by CO adsorption followed by FTIR spectroscopy in a Nicolet Nexus 470 spectrophotometer equipped with an environmentally controlled Spectra Tech DRIFT cell with ZnSe windows. About 0.025 g of the sample was packed in the sample holder and pretreated in situ under air flow (30 cm^3 min^{-1}) at 300 °C for 1 h. After this treatment the sample was purged with He for 1 h and cooled to room temperature in the same gas atmosphere before admittance for 5 min of 2000 ppm CO diluted in helium. Afterwards, pure helium was allowed to flow in the system to eliminate the residual CO gas. Spectra were collected from 256 scans with a resolution of 4 cm^{-1} at different temperatures and in all cases difference spectra were obtained by making reference to the freshly calcined solid prior to CO adsorption. The spectrum of dry KBr was taken for IR single-beam background subtraction.

2.3. Catalytic activity

The selective oxidation of CO in H_2 stream was carried out in a fixed-bed reactor system (RIG-100). Prior to catalytic run all catalyst samples were pretreated in situ in air flow at 300 °C for 1 h and cooled to room temperature in He. The catalytic reaction was studied in the temperature range RT–250 °C. The feed gas composition was 1% CO, 1% O_2, 50% H_2 and balance

He with a total flow of 120 $cm^3\,min^{-1}$ and a GHSV = 72,000 h^{-1}. Product and reactant analysis was carried out by gas chromatography (TCD) with a Carboxen 1000 (Supelco) packed column. The effect of CO_2 and H_2O (10 vol.%) in the activity was examined independently and simultaneously by addition of each or both components to the feed. The CO conversion and selectivity were calculated as follows:

$$\text{CO conversion}\,(\%) = \frac{[CO]_{in} - [CO]_{out}}{[CO]_{in}} \times 100 \quad \text{and}$$

$$\text{Selectivity}\,(\%) = \frac{0.5([CO]_{in} - [CO]_{out})}{[O_2]_{in} - [O_2]_{out}} \times 100$$

3. Results and discussion

Textural features of supports and catalysts are tabulated in Table 1. As it can be observed specific surface area (S_{BET}) of the ceria support synthesized in this work (SCe) is 6 times higher than the one presented by the reference ACe ceria. The total pore volume (V_p) follows the same trend. According to these observations the mean crystal size of the CeO_2 determined by the Rietveld method in the SCe sample is about 5 times lower than the one calculated for the ACe reference sample (Table 1). When copper is incorporated to the support a decrease in the specific surface area and the pore volume is observed as a function of the loading. This phenomenon can be attributed to a blockage of the pores of the support by copper. On the other hand, a slight increase in the CeO_2 crystal size was observed for all samples as the copper content in the catalyst increased.

XRD patterns showed the fluorite type structure of ceria in supports and catalysts (not shown). The refinement of the crystal structure by Rietveld showed for the SCe support an increase in the cell parameter of the CeO_2. Such modification has been reported to occur as the crystal size decreases [23] which is the case for these samples (Table 1). For the catalysts, the identification of small diffraction lines corresponding to the CuO phase was only possible in the 6CuACe, 9CuACe and 9CuSCe catalysts, while no evidence of this phase was observed in the 3CuACe, 3CuSCe and 6CuSCe samples. Fig. 1 shows as an example the XRD patterns of the CuSCe series catalysts. This result suggests that copper species on the support are either highly dispersed or as small crystals whose size is below the resolution limit of the technique. On the other hand, a slight contraction in the cell parameter of the CeO_2 was observed by Rietveld for ACe and SCe supports as copper is incorporated. As an example for the CuSCe series, the cell parameter changes from 0.54156(±5) nm to 0.54139(±5) nm in the 6CuSCe catalyst.

Table 1
Characterization results of supports and catalysts

Sample	S_{BET} ($m^2\,g^{-1}$)	Vp ($cm^3\,g^{-1}$)	Cu content (wt.%)[a]	Mean crystal Size (nm)[b]
ACe	26	0.12	–	37.2 ± 0.2
SCe	161	0.24	–	7.5 ± 0.05
3CuACe	24	0.12	2.9	37.2 ± 0.2
6CuACe	22	0.11	5.2	37.8 ± 0.2
9CuACe	21	0.11	7.8	38.4 ± 0.2
3CuSCe	145	0.23	3.0	7.6 ± 0.05
6CuSCe	136	0.22	5.9	7.7 ± 0.05
9CuSCe	125	0.20	8.7	7.6 ± 0.05

[a] Determined by EDS analysis.
[b] Determined by XRD using the Rietveld method.

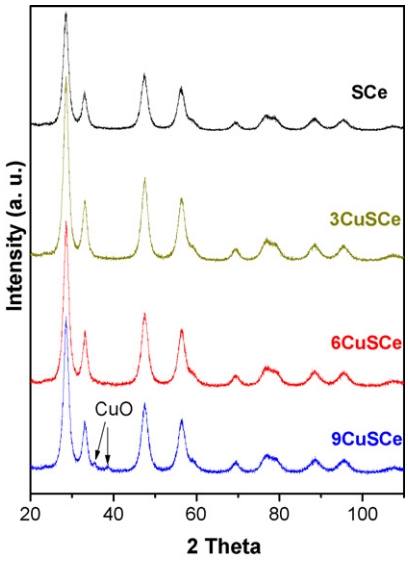

Fig. 1. XRD patterns of *X*CuSCe catalysts as a function of the copper loading (*X* = 3–9 wt.%). SCe refers to the CeO_2 synthetized in this work.

HRTEM characterization of supports and catalysts showed that the mean crystal size of CeO_2 in the SCe support was below 10 nm, while in the case of the ACe it was above 25 nm. These results are in good agreement with those obtained by XRD (Table 1). Identification of the copper phase by HRTEM in the CuSCe catalysts was extremely hard. Evidence of some CuO crystals only in the samples with high copper content was obtained. Fig. 2 shows a typical image of the 6CuSCe catalyst, were (1 1 1) planes of CeO_2 crystals with interplanar distance

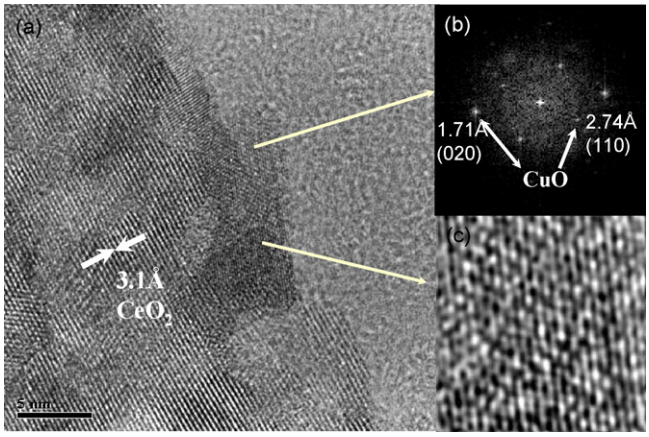

Fig. 2. HRTEM characterization of the 6CuSCe catalyst. (a) Typical image showing CeO_2 crystals, (b) Fourier pattern associated with a thin CuO crystal, and (c) Image reconstruction from the fourier pattern.

$d = 0.310$ nm are clearly identified. The presence of the CuO phase was evidenced by indexing the fourier pattern (inset b) associated with a thin crystal showing a smaller interplanar distance (0.274 nm). It is important to mention that the presence of copper in this catalyst and others where apparently no copper oxide crystals were evident in the image was confirmed by chemical mapping using EELS technique. This supports the idea that highly dispersed copper oxide crystals are present in the CuSCe catalysts.

The H_2-TPR profiles of the catalysts are shown in Fig. 3. A well-defined two-step reduction profile is observed for all CuSCe catalysts indicating the existence of at least two copper species. Two reduction peaks are observed roughly in the range 80–250 °C. The position and the relative intensity of these peaks changed as a function of the copper content in the catalyst. In the 3CuSCe sample the maxima of the peaks were at ca. 125 and 200 °C whereas in the 6CuSCe and 9CuSCe catalysts these peaks (mostly the first one) shifted to lower temperatures. On the other hand, the relative intensity of the low temperature peak increased in the 6CuSCe catalyst while this was the case for the high temperature peak in the 9CuSCe catalyst. Samples supported on the commercial ceria (ACe), presented broad TPR profiles with reduction peaks at much higher temperatures compared to the CuSCe series. The 9CuACe catalyst showed a maximum in H_2 consumption at ca. 270 °C. According to the literature, reduction of copper supported on CeO_2-based materials is characterized by reduction peaks appearing at low and high temperature which are attributed to reduction, respectively, of more or less dispersed CuO species over the CeO_2 surface [24–27]. The relative intensity of the peaks and their position is related to the copper loading. Wrobel et al. [28] reported for Cu/CeO_2 systems a reduction process at quite low temperature (127–157 °C) assigned to highly dispersed CuO in contact with ceria particles. Larger CuO particles were reduced at higher temperatures (200 °C). On their side, Kundakovic et al. [29] assigned to peaks at 180 °C the reduction of isolated ions interacting strongly with the support. Although reduction temperatures are lower compared to those reported in the literature, we can assume the presence of highly dispersed CuO clusters and somewhat larger CuO particles which are characterized by reduction peaks below 200 °C in our CuSCe catalysts. This assumption is also supported by the XRD and HRTEM results previously presented. On the contrary, the TPR behavior of the CuACe series points out to the presence of bulky like CuO particles which reduced at higher temperatures. This fact is understandable because of the low surface area of the support ($26\ m^2\ g^{-1}$). The temperature of the broad reduction peak of 9CuACe catalyst was close to that of the CuO bulk used as reference to calibrate de TCD signal (315 °C).

Quantitative analysis showed for CuSCe catalysts that the actual hydrogen consumption is about 2 times higher than the one predicted from the stoichiometry $Cu^{2+} \rightarrow Cu^0$. For the CuACe series catalysts it was not the case since the amount of H_2 to complete the reduction process was near the predicted one. Reports in the literature have shown that for metals supported on CeO_2 the metal promotes the surface reduction of ceria at lower temperature [17]. On the other hand, the redox properties of CeO_2 are enhanced when the crystal size of ceria decreases. Taking this into account, the enhanced H_2 consumption of the CuSCe catalysts may be understood as the synergic combination of the presence of small CeO_2 crystals

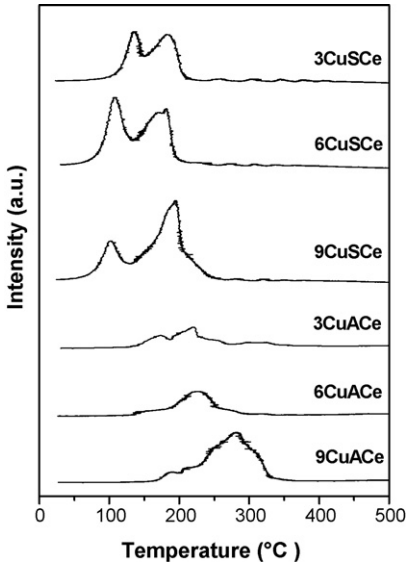

Fig. 3. TPR profiles of CuSCe and CuACe at different copper loading (3–9 wt.%).

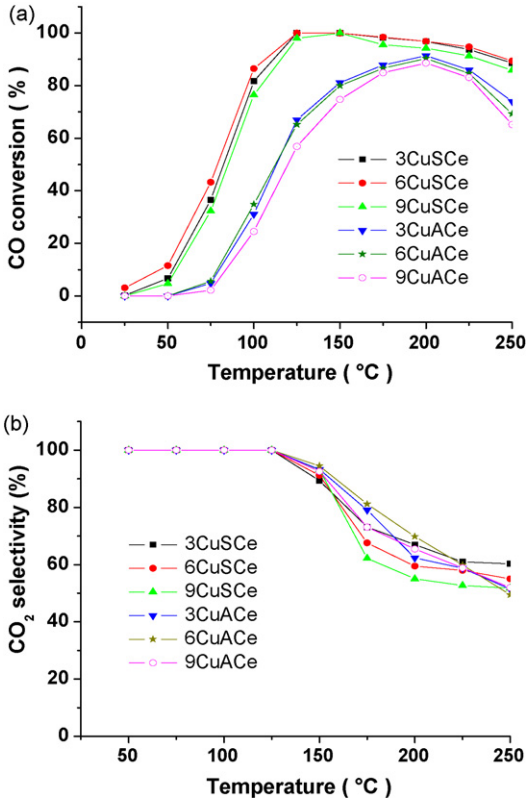

Fig. 4. CO oxidation in the presence of excess H_2 studied on CuSCe and CuACe catalysts. Evolution of (a) the CO conversion and (b) the CO_2 selectivity as a function of the reaction temperature. Feed composition (v/v): 1% CO:1% O_2:50% H_2: balance He. GHSV = 72,000 h^{-1}, $W/F = 0.05$ g s cm^{-3}.

in contact with highly dispersed copper species which promote a higher surface reduction of the CeO_2. The amount of surface oxygen available for reduction is then controlled by the crystal size of CeO_2 and the dispersion of copper species.

The catalytic activity for CO oxidation in the presence of an excess of H_2 as a function of the reaction temperature is presented in Fig. 4 for both series of catalysts where the evolution of the CO conversion (Fig. 4a) and the corresponding selectivity to CO_2 (Fig. 4b) are displayed. The first observation is that CuSCe catalysts are more active than the CuACe ones. The 6CuSCe catalyst which is slightly the most active of the series (mostly at low temperature) presented a sharp increase in CO conversion above 50 °C with 100% conversion at 125 °C. Total conversion of CO was achieved by the three catalysts of the CuSCe series at the same temperature. The CO conversion in CuACe samples was only about 60% at 125 °C with a maximum conversion around 90% at 200 °C. It is important to note that above a reaction temperature of 150 °C in the CuSCe catalysts and above 200 °C in the CuACe catalysts, the CO conversion decreases. Concerning the selectivity (Fig. 4b) at 125 °C all set of catalysts presented 100% selectivity to CO_2, however, it is important to remind that the CuSCe catalysts presented 100% conversion of CO at this temperature while for the CuACe catalysts it was only about 60%. At temperatures higher than 125 °C a more or less pronounced diminution of the selectivity depending on the catalyst takes place. The diminution of the selectivity to CO_2 is clearly related to the $H_2 + O_2$ reaction which is favored at high temperatures. The presence of H_2O in the reaction products was detected from 150 °C. Methane formation was not observed under our experimental conditions.

The effect of CO_2 and H_2O in the reactant mixture (RM) was studied using the most active catalyst (6CuSCe). The activity (Fig. 5a) and selectivity (Fig. 5b) curves are issued from independent experiments in the presence either of CO_2 (RM + CO_2) or H_2O (RM + H_2O) and in the presence of both components (RM + CO_2 + H_2O). For comparison, the corresponding curve obtained without CO_2 and H_2O in the reaction mixture (RM) is also presented. The addition of CO_2 and H_2O to the feed leads in general to a diminution of the catalyst activity although this diminution is more pronounced in the presence of H_2O, as it can be observed in Fig. 5a. While in the absence of these molecules a 50% conversion of CO is achieved at T_{50} = 75 °C, the same conversion is obtained at 92 °C in the presence of CO_2 and at 115 °C in the presence of H_2O. When both components are present T_{50} is unchanged (115 °C) and the maximum CO conversion is around 95% at 150 °C. On the other hand, the effect of both components is totally reversible since the activity of the catalyst is fully restored as CO_2 and H_2O are eliminated from the feed (Fig. 5a, experiments RM + X (R) where X is CO_2 and/or H_2O). The competitive adsorption of the CO_2 and the blockage of active sites by the H_2O molecules have been used as argument to explain the decrease of the catalytic activity [16] in the selective CO oxidation. The selectivity, Fig. 5b, even in the presence of both components (CO_2 and H_2O), remains unchanged (100%) for reaction temperatures lower than 125 °C. At higher temperatures, a diminution is observed being this diminution more

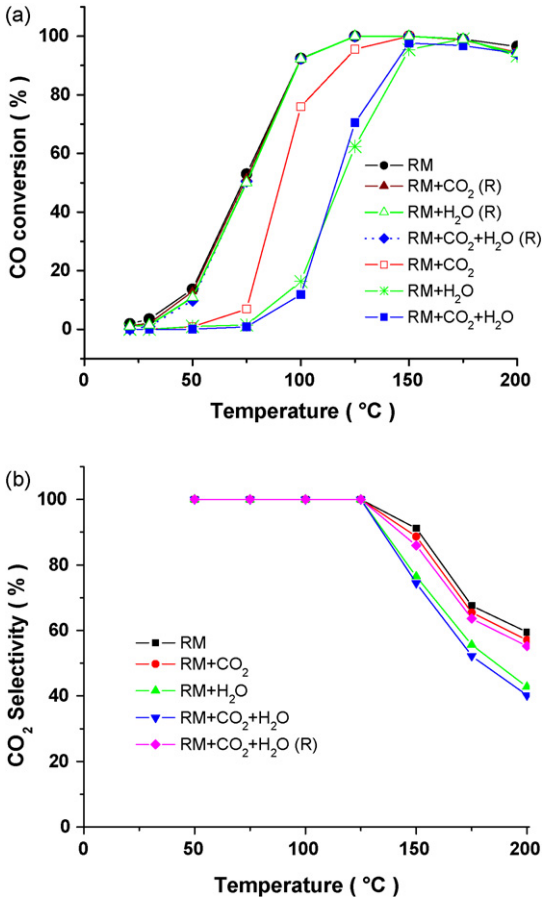

Fig. 5. Effect of CO_2 and H_2O addition (10 vol.% each) to the reactant mixture (1% CO:1% O_2:50% H_2: balance He) on (a) the catalytic activity and (b) the CO_2 selectivity. RM: Reactant mixture, RM + X where X is CO_2 and/or H_2O, and RM + X (R) where (R) identifies the run after elimination of CO_2 and/or H_2O from the feed.

pronounced when H_2O is present in the feed (55% at 175 °C with a 95% CO conversion). On the other hand, elimination of both components led to almost a total recovery of the initial selectivity values (Fig. 5b, RM + CO_2 + H_2O (R) run).

Comparison of the performance of CuSCe series catalysts with some catalytic systems in the literature may be attempted. Regarding Pt supported catalysts, Igarashi et al. [13] reported for a 5.9% Pt/Mordenite catalyst (W/F = 0.06 g s cm^{-3}, 1 vol.% CO and 1 vol.% O_2, balance H_2) at 200 °C a CO conversion of 63% with a selectivity of 57%. Under our experimental conditions (W/F = 0.05 g s cm^{-3}, 1 vol.% CO, 1 vol.% O_2 and 50 vol.% H_2, balance He) at 150 °C the 6CuSCe catalyst displayed a CO conversion of 100% with a selectivity of 92%. At 200 °C a slightly lower CO conversion (97%) was obtained with 60% selectivity. Based on these results the CuSCe catalysts seem to be more active and selective than Pt/Mordenite while operating at lower temperatures. CuO-CeO_2 catalysts prepared by the urea gelation/co-precipitation method were studied by Liu et al. [30]. The authors reported a 100% selectivity for CO conversions around 30 and 90% at 75 and 125 °C, respectively (reaction conditions: 1 vol.% CO, 1 vol.% O_2, 50 vol.% H_2 balance He and contact time W/F = 0.045 g s cm^{-3}). In the presence of CO_2 and H_2O

(20 vol.% CO_2 and 10 vol.% H_2O) the CO conversion and selectivity were around 35 and 65%, respectively, at 165 °C. In comparison, the 6CuSCe catalyst in this work, at the same reaction temperatures (75 and 125 °C) and similar experimental conditions (1 vol.% CO, 1 vol.% O_2, 50 vol.% H_2 balance He and contact time W/F = 0.05 g s cm^{-3}) is more active (43 and 100% CO conversion, respectively) with 100% selectivity. In the presence of 10 vol.% CO_2 and 10 vol.% H_2O, CO conversion and selectivity for this catalyst are 95 and 50%, respectively at 175 °C. Sedmak et al. [31] on their side, studying a nanostructured $Cu_{0.1}Ce_{0.9}O_{2-y}$ catalyst prepared by a sol-method, reported for the PROX reaction at 90 °C a reaction rate of 2.7×10^{-6} $mols^{-1}$ g_{cat}^{-1}. At this temperature the CO conversion is around 60% and the selectivity is 100% for a reaction mixture consisting of CO, O_2 (λ = 2.5), 50% H_2, balance He. For similar copper content and reaction conditions, the 9CuSCe catalyst in this work showed at 100 °C a CO conversion around 76% with 100% selectivity. The observed reaction rate at this temperature is 5.3×10^{-6} mol_{CO} s^{-1} g_{cat}^{-1}. Avgouropoulos et al. [15] reported for a co-precipitated 5.7 wt.% CuO-CeO_2 catalyst at 210 °C (1 vol.% CO, 1.25 vol.% O_2 and 50 vol.% H_2 in He, and W/F ratio of 0.03 g s cm^{-3}) the highest CO conversion (96%) with a 50% selectivity. Selectivity values >95% were obtained in the temperature range 75–140 °C where CO conversion ranged from 15 to 80%. The reaction rate at 75 °C is 2.28×10^{-6} mol_{CO} s^{-1} g_{cat}^{-1}. In the presence of 15 vol.% CO_2 in the feed the observed rate at 100 °C was 2.16×10^{-6} mol_{CO} s^{-1} g_{cat}^{-1}. For similar copper content and experimental conditions, the 6CuSCe catalyst of this work displayed 100% CO conversion and 100% selectivity at 125 °C. The calculated reaction rate at 75 °C is 3.01×10^{-6} mol_{CO} s^{-1} g_{cat}^{-1} while in the presence of 10 vol.% CO_2 the reaction rate at 100 °C is 5.28×10^{-6} mol_{CO} s^{-1} g_{cat}^{-1}.

We can conclude from this comparison that at least for similar reaction conditions and copper content, the CuSCe catalysts studied in this work are more active than the reported ones while keeping a good selectivity.

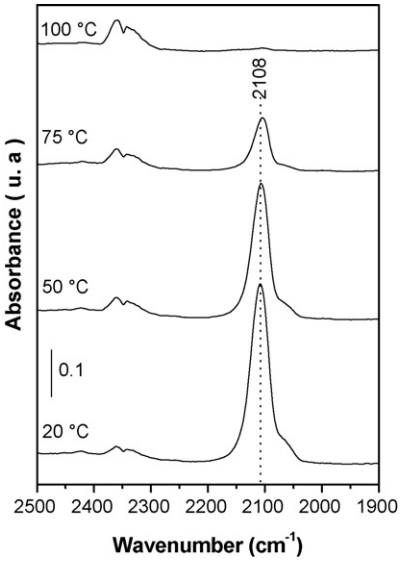

Fig. 6. CO adsorption on 6CuSCe catalyst as a function of temperature followed by DRIFT.

In order to know about the copper species present in the catalysts CO adsorption was done and followed by DRIFT. Fig. 6 displays the spectral region 1900–2400 cm^{-1} for the freshly in situ calcined 6CuSCe catalyst. At room temperature one intense band is observed at 2108 cm^{-1} with a shoulder at lower frequencies (ca. 2060 cm^{-1}) as well as a small signal from CO_2 gas around 2350 cm^{-1}. As the temperature increases a diminution of the intensity of the main band is observed with, at the same time, an increase in the CO_2 signal. The CO band practically disappeared at 100 °C. Similar behavior was observed for the other catalysts of the CuSCe series. On the other hand, the catalyst supported on commercial ceria (6CuACe) showed absorption band located at ca. 2101 cm^{-1} of lower intensity compared to that observed for the 6CuSCe sample. This band practically disappeared upon heating at 75 °C (not shown). The lower intensity of the carbonyl band observed for 6CuACe catalysts can be understood taking into account the poorer dispersion of the copper phase on the low area support as evidenced by the XRD and TPR experiments. The characteristic linear carbonyl stretching absorption bands of CO on copper appear in the range 2050–2160 cm^{-1}. The Cu^0–carbonyls are usually detected below 2110 cm^{-1} and variations in their position are related to changes in the nature of the exposed metallic copper faces [32] and, in the case of supported catalysts, to the interaction of the particles with the support [33]. Bands associated with Cu^+–CO are usually observed in the range 2115–2140 cm^{-1} but in some cases when copper is highly dispersed, they can be found in the region where the Cu^0–CO species absorbs [34]. On these bases, it is clear from the DRIFT experiments that reduction of the copper phase takes place readily at room temperature in the presence of CO. On the basis of the band position, assignment to CO adsorbed on reduced Cu^0 sites would be adequate; an alternative assignment might be made assuming interactions with the support as proposed by Martínez-Arias et al. [35]. Bands of carbonyl species adsorbed on copper sites on ceria-related oxides have been observed around 2110 cm^{-1}. Although this frequency is somewhat low for a cationic copper species since it is found in the limit region where Cu^0–CO appear, it has been attributed to Cu^+–carbonyls. Discrimination between Cu^0–CO and Cu^+–CO has been done on the basis of the relatively high thermal stability of the latter [36]. In this sense the thermal stability of the CO band (Fig. 6) supports the assumption of the occurrence of Cu^+ species in the catalysts, although reduced copper species $Cu^{\delta+}$ species, where $1 > \delta > 0$ might not be ruled out.

4. Conclusions

In this study high surface area CeO_2 with a crystal size around 7 nm was synthesized by the surfactant route and used as support to prepare CuO/CeO_2 catalysts with copper content in the range 3–9 wt.% identified as CuSCe catalysts. Reference catalysts were prepared using a low surface area commercial ceria (CuACe catalysts). CuSCe catalysts presented highly

dispersed copper species in strong interaction with nanosized CeO_2 crystals as evidenced by XRD, HRTEM and TPR experiments. In particular quantitative measurements of H_2 consumed during TPR experiments put in evidence the synergic interaction between small CeO_2 crystals and highly dispersed copper species which promoted a surface reduction of the CeO_2 at lower temperature. This enhanced redox properties of the CuO_x–support interface sites at low temperature, not present in the CuACe catalysts, play a fundamental role in the catalytic behavior for the CO oxidation in presence of excess H_2 (PROX). The catalyst presented an excellent catalytic activity with 100% conversion of CO and 100% selectivity to CO_2 up to 125 °C. Up to this temperature, the presence of CO_2 and H_2O in the reaction mixture provoked a diminution of the CO conversion in the catalyst while keeping 100% selectivity. Above this reaction temperature the catalyst recovered its activity (around 95% CO conversion) showing 74% selectivity at 150 °C. The effect of these molecules was reversible since the activity and selectivity of the catalyst is practically restored upon elimination of these components. Partially reduced Cu^+ species seem to be present in the catalysts according to CO adsorption followed by DRIFT.

Acknowledgments

This research was supported by CONACYT (42666F) and PAPIIT (IN-117706). Technical help from Manuel Aguilar Franco (XRD) and Luis Rendón LCM-IF (HRTEM) is also acknowledged.

References

[1] D. Megede, J. Power Sources 106 (2002) 35.
[2] L. Carrette, K.A. Friedrich, U. Stimming, Chem. Phys. Chem. 1 (2000) 162.
[3] D. Tibiletti, E.A. Bart de Graaf, S.P. Teh, G. Rothenberg, D. Farrusseng, C. Mirodatos, J. Catal. 225 (2004) 489.
[4] A. Manasilp, E. Gulari, Appl. Catal. B: Environ. 37 (2002) 17.
[5] M. Haruta, Cattech 6 (2002) 102.
[6] R.J.H. Grisel, B.E. Nieuwenhuys, J. Catal. 199 (2001) 48.
[7] G. Avgouropoulos, T. Ioannides, Ch. Papadopoulou, J. Batista, S. Hocevar, H.K. Matralis, Catal. Today 75 (2002) 157.
[8] G.K. Bethke, H.H. Kung, Appl. Catal. A 194–195 (2000) 43.
[9] M.M. Schubert, V. Plzak, J. Garche, R.J. Behm, Catal. Lett. 76 (2001) 143.
[10] S.M. Zhang, W.-P. Huang, X.-H. Qiu, B.-Q. Li, X.-C. Zheng, S.H. Wu, Catal. Lett. 80 (2002) 41.
[11] D.H. Kim, M.S. Lim, Appl. Catal. A 224 (2002) 27.
[12] M.J. Kahlich, H.A. Gasteiger, R.J. Behm, J. Catal. 171 (1997) 93.
[13] H. Igarashi, H. Uchida, M. Suzuki, Y. Sasaki, M. Watanabe, Appl. Catal. A 159 (1997) 159.
[14] W.H. Cheng, React. Kinet. Catal. Lett. 58 (1996) 329.
[15] G. Avgouropoulos, T. Ioannides, H.K. Matralis, J. Batista, S. Hocevar, Catal. Lett. 73 (2001) 33.
[16] G. Avgouropoulos, T. Ioannides, Appl. Catal. A: General 244 (2003) 155.
[17] A. Trovarelli (Ed.), Catalysis by Ceria and Related Materials, Catalytic Science Series, vol. 2, Imperial College Press, 2002.
[18] E. Rocchini, A. Trovarelli, J. Llorca, G.W. Graham, W.H. Weber, M. Maciejewski, A. Baiker, J. Catal. 194 (2000) 461.
[19] J.E. Spainier, R.D. Robinson, F. Zhang, S. Chan, I.P. Herman, Phys. Rev. B 64 (2001) 245407.
[20] A. Martínez-Arias, M. Fernández-García, O. Gálvez, J.M. Coronado, J.A. Anderson, J.C. Conesa, J. Soria, G. Munuera, J. Catal. 195 (2000) 207.
[21] D.M. Lyons, K.M. Ryan, M.A. Morris, J. Mater. Chem. 12 (2002) 1204.
[22] J. Rodríguez-Carvajal, FullProf, web site: ftp://ftp.cea.fr/pub/llb/divers/fullprof.2k.
[23] F. Zhang, S.W. Chan, J.E. Spanier, E. Apak, Q. Jin, R.D. Robinson, I.P. Herman, Appl. Phys. Lett. 80 (1) (2002) 127.
[24] M. Manzoli, R.D. Monte, F. Boccuzzi, S. Coluccia, J. Kaspar, Appl. Catal. B 61 (2005) 192.
[25] M.F. Luo, Y.J. Zhong, X.X. Yuan, X.M. Zheng, Appl. Catal. A Gen. 162 (1997) 121.
[26] G. Sedmak, S. Hocevar, J. Levec, J. Catal. 222 (2004) 87.
[27] P. Ratnasamy, D. Srinivas, C.V.V. Satyanarayana, P. Manikandan, R.S.S. Kumaran, M. Sachin, V.N. Shetti, J. Catal. 221 (2004) 455.
[28] C. Wrobel, A. Lamonier, A.D. Bennani, A. Huysser, J. Aboukais, J. Chem. Soc. Faraday Trans. 92 (1996) 20001.
[29] Lj. Kundakovic, M. Flytzani-Stephanopoulos, Appl. Catal. A Gen. 171 (1998) 13.
[30] Y. Liu, Q. Fu, M.F. Stephanopoulos, Catal. Today 63–95 (2004) 241.
[31] G. Sedmak, S. Hocevar, J. Levec, J. Catal. 213 (2003) 135.
[32] P. Hollins, Surf. Sci. Rep. 16 (1992) 51.
[33] A. Martínez-Arias, M. Fernández-García, J. Soria, J.C. Conesa, J. Catal. 182 (1999) 367.
[34] A.R. Balkenende, C.J.G. van der Grift, E.A. Meulenkamp, J.W. Geus, Appl. Surf. Sci. 68 (1993) 161.
[35] A. Martínez-Arias, R. Cataluña, J.C. Conesa, J. Soria, J. Phys. Chem. B 102 (1998) 809.
[36] A. Martínez-Arias, M. Fernández-García, A.B. Hungría, A. Iglesias-Juez, O. Gálvez, J.A. Anderson, J.C. Conesa, J. Soria, G. Munuera, J. Catal. 214 (2003) 261.